The Calculation of Transonic Rotor Noise

Hans R. Aggarwal*
University of Santa Clara, Santa Clara, California

Introduction

An accurate prediction of the high-speed impulsive rotor noise is very difficult since the noise field depends on many complex factors, such as the complicated rotating blade geometry, the existence of a large transonic disturbance field surrounding the blade, and the appearance of a persistent shock in the outer regions of the blade due to intense compressibility effects. In their experiments Boxwell et. al.[1] noted a "delocalization phenomenon" at high tip Mach numbers in which the far-field acoustic waveform changes from near symmetric triangular wave to a saw-toothed pulse. A logical explanation of this phenomenon was given by Isom.[2] Using a second-order potential equation describing both the acoustic and the flow fields of a hovering rotor he showed that, depending upon blade rotational velocity and the size of certain local flow quantities, the type of the governing equation may change from elliptic to hyperbolic. A consequence of this transition is that a shock formed on the blade escapes to the acoustic far field, thereby implying that local aerodynamic nonlinearities, the quadrupoles, strongly influence the acoustic waveform.

Recently, Schmitz and Yu,[3] in order to include the local aerodynamic nonlinearities in their calculation to capture the acoustic shock, extended the base support region $d\Sigma$ [see Eq. (4) below] for the integration of their model quadrupole source integral developed earlier.[4,5] Using a planform integration technique they computed the pressure-time history curves for a 1/7-scale untwisted UH-1H model rotor, NACA 0012 airfoil, in hover, for tip Mach numbers from 0.8 to 0.9. By comparing these results with those previously obtained by them experimentally by running the model rotor at near zero thrust and high subsonic tip Mach numbers in an anechoic hover chamber, Schmitz and Yu[3,6] showed that good agreement existed between the theoretical and experimental waveforms for tip Mach numbers from 0.8 to 0.9. They observed a good correlation between peak negative amplitudes at tip Mach number, $M_T = 0.88$, while they noted that their theory overpredicted the measured peak negative amplitudes for $M_T = 0.9$.

A study of the Schmitz-Yu computation revealed some of the assumptions they had implicitly made in their work. To better understand their computations, the hover case of the model rotor studied by these authors was recomputed without the implicit assumptions, using the same theory and velocity field as used by them. The results of this computation are given in this Note. These results show that the Schmitz-Yu computations are very much base-support area dependent. Some other differences between the two computations also were found and are discussed herein.

The Quadrupole Integral

The quadrupole source integral is given by[7]:

$$I = \frac{\partial^2}{\partial x_i \partial x_j} \int_{WS} \left[\frac{T_{ij}}{R\,|1 - M_R|} \right] d\eta \tag{1}$$

where x_i represents the position of the observer in a reference frame fixed in space: WS the whole space surrounding the rotor; T_{ij} the Lighthill stress tensor; $R = |x - y|$; y the source position in space-fixed coordinates; M_R the local Mach number in the radiation direction; $d\eta$ the differential volume element in blade-fixed reference frame; the notation [ ] indicates that the intergrand is evaluated at the retarded time $\tau = t - R/c$, where t is time and c the local velocity of sound. For an in-plane far-field radiation Schmitz et al.[4,5] approximated the quadrupole integral by a model integral given by

$$I_{\text{model}} = \frac{1}{c_0^2} \frac{\partial^2}{\partial t^2} \int_{WS} \left[\frac{T_{RR}}{R\,|1 - M_R|} \right] d\eta \tag{2}$$

where

$$T_{RR} = \rho_0 u^2 \left[\cos^2\theta + \frac{\gamma - 1}{2} \left(\frac{\omega r}{c_0} \right)^2 \right] \tag{3}$$

ρ_0 is the density, c_0 the velocity of sound in the undisturbed medium, u the perturbation velocity along the blade chord, θ the angle between the direction of u and the radiation direction at any point, ω the rotational velocity of the blade, and r the radial (spanwise) coordinate. In order to avoid integrating around the singularities given by the equation $M_R = 1$, Schmitz and Yu used a planform method to evaluate the model integral, Eq. (2), which in a planform reference frame may be written as

$$I_{\text{model}} = \frac{1}{c_0^2} \frac{\partial^2}{\partial t^2} \int_{WS} \left[\frac{J T_{RR}}{R} \right] dF\, d\Sigma \tag{4}$$

where J is the Jacobian of transformation defined by

$$J = 1/(\Lambda\,|\nabla f|) \tag{5}$$

$$\Lambda = (1 + M_n^2 - 2M_n \cos\theta)^{1/2} \tag{6}$$

[see Eqs. (6-8) in Ref. 8]. M_n, in the light of assumptions made in the derivation of quadrupole model, Eq. (3), is the local Mach number u/c; $f(y, \tau) = 0$ is the equation of the blade surface; Σ is the surface generated by Γ, the curve of in-

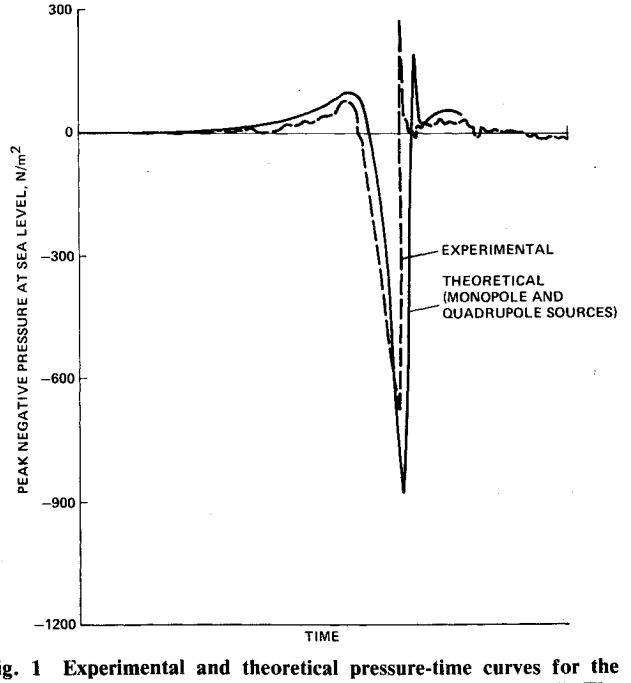

Fig. 1 Experimental and theoretical pressure-time curves for the model rotor in hover, in-plane, $r_{obs}/R_0 = 3.0$, $M_T = 0.9$ (Ref. 3). The time scale in this figure is approximately the same as in Figs. 2 and 3.

Received July 18, 1983; revision received Oct. 27, 1983. Copyright © American Institute of Aeronautics and Astronautics, Inc., 1983. All rights reserved.

*Senior Research Associate, Department of Mechanical Engineering.

teraction of the blade surface $f=0$ with the collapsing sphere $\tau=t-R/c$; and dF is the differential element normal to $d\Sigma$.

Results and Discussion

The experimental and theoretical curves of Schmitz and Yu for an in-plane case of the model rotor in hover $r_{obs}/R_0=3.0$, where r_{obs} is the distance of the observer from the hub and R_0 is the blade span, and $M_T=0.9$, Refs. 3 and 6, are given in Fig. 1. It is observed that Schmitz and Yu assumed θ as being a constant in computing the theoretical curve. They also took $J=1$ in this calculation, thereby neglecting the effect of the Jacobian on the computation. The pressure-time history curves for the hover case considered by Schmitz and Yu, using their theory and velocity field, allowing θ to be a variable, and including the effect of the Jacobian for three different base-support areas A, B, and C, are given in Fig. 2. These base-support areas are among the ones considered by Schmitz and Yu in their works and are as defined as

A: $0.75\le r/R_0\le 1$, $0\le x/C_0\le 1$

B: $0.75\le r/R_0\le 1.22$, $0\le x/C_0\le 1$

C: $0.75\le r/R_0\le 1.22$, $0\le x/C_0\le 3.5428$

where x is the chordwise coordinate and C_0 is the blade chord. From this figure one sees that the Schmitz-Yu pressure-time curves are very much base-support area dependent. One also notes that the peak amplitude given by the dotted line curve is 11-15% larger than the one given by the solid line curve which, in turn, is 53% larger than its value given by the experimental curve in Fig. 1. Compared to the approximately 29% overprediction in the peak amplitude as reflected by the theoretical curve in Fig. 1, the above result shows that the Schmitz-Yu theory greatly ovrpredicts the peak negative pressures compared to that given by the experiment. Also, the after-suction recovery in the solid line curve now is substantially eroded and is much less like the one shown by the theoretical curve in Fig. 1. It is noted that the effect of the Jacobian on the above computation was found to be small. The smallness of the effect may be due to the plane rectangular geometry of the rotor blade employed in the example. It improved the peak negative amplitudes by about 5%, but was seen to deteriorate the after-suction recovery somewhat further.

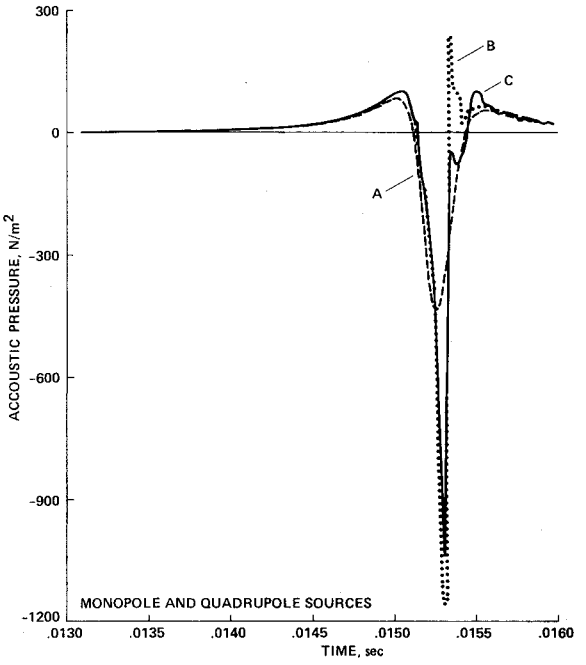

Fig. 2 Modified pressure-time curves for the model rotor in hover, in-plane, $r_{obs}/R_0=3.0$, $M_T=0.9$ for base-support areas A, B, and C.

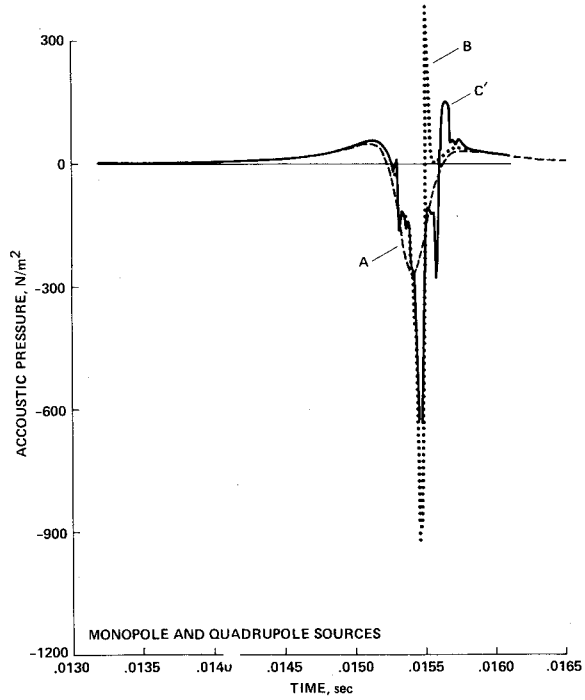

Fig. 3 Modified pressure-time curves for the model rotor in hover, in-plane, $r_{obs}/R_0=3.0$, $M_T=0.88$ for base-support areas A, B, and C′.

From the above discussion, it may follow that as the base-support area increases, the pressure-time curve may tend to a computationally unique solution with a peak negative amplitude comparable to that given by the experimental curve in Fig. 1. To decide this issue, pressure-time curves for tip Mach number $M_T=0.88$ were computed for the model rotor for the same parameters and base-support areas A, B and C′ where C′ is defined as C′: $0.75\le r/R_0\le 1.22$, $0\le x/C_0\le 1.8521$. They are displayed in Fig. 3, which shows that with increasing base-support area, the pressure-time curve may become computationally unstable.

While, as also remarked by Schmitz and Yu,[3,6] the knowledge of an accurate velocity field surrounding the blade is necessary to predict the far-field transonic noise correctly, it appears that the one-dimensional quadrupole source model, Eq. (3), is not adequate in itself and needs some improvement. It may need the inclusion of the other velocity components and/or the curvature of the airfoil and other blade geometry and/or relaxing the condition on the retarded time which is assumed to be the same for longitudinal quadrupole sources on any line perpendicular to the chord line of the airfoil.

Acknowledgments

This research was carried out under NASA Grant NCC2-191 with the University of Santa Clara, Santa Clara, Calif. The author is grateful to Dr. Sanford S. Davis of NASA Ames Research Center for the support.

References

[1] Boxwell, D. A., Yu, Y. H., and Schmitz, F. H., "Hovering Impulsive Noise: Some Measured and Calculated Results," *Vertica*, Vol. 3, 1979, pp. 35-45.

[2] Isom, M. P., "Acoustic Shock Waves Generated by a Transonic Helicopter Blade," Paper 80-63 presented at the 36th Annual Forum of the American Helicopter Society, Washington, D.C., May 1980.

[3] Schmitz, F. H. and Yu, Y. H., "Transonic Rotor Noise—Theoretical and Experimental Comparisons," *Vertica*, Vol. 5, 1981, pp. 55-74.

[4] Schmitz, F. H. and Yu, Y. H. "Theoretical Modeling of High-Speed Helicopter Impulsive Noise," *Journal of the American Helicopter Society*, Vol. 24, Jan. 1979, pp. 10-19.

[5]Yu, Y. H., Caradonna, F. X., and Schmitz, F. H., "The Influence of the Transonic Flow Field on High-Speed Helicopter Impulsive Noise," Paper 58, presented at the 4th European Rotorcraft and Powered Lift Aircraft Forum, Stresa, Italy, Sept. 1978.

[6]Schmitz, F. H. and Yu, Y. H., "Helicopter Impulsive Noise: Theoretical and Experimental Status," NASA TM 84390, USA AVRADCOM TR 83-A2, Nov. 1983.

[7]Goldstein, M. E., *Aeroacoustics,* McGraw-Hill Book Co., New York, 1976, p. 119.

[8]Farassat, F., "Linear Acoustic Formulas for Calculation of Rotating Blade Noise," *AIAA Journal,* Vol. 19, Sept. 1981, pp. 1122-1130.

Axisymmetric Nonconical Supersonic Potential Flow with Embedded Subsonic Regions

M. J. Siclari*
Grumman Aerospace Corporation
Bethpage, New York

Introduction

FREESTREAM conditions in the 1.2-1.6 Mach number range can generate locally subsonic radial and total Mach numbers in the vicinity of fuselage-canopy and wing leading-edge regions. In this low supersonic range traditional transonic methods should be applicable. Unfortunately, transonic meshes are not well suited to attached bow shock computations and if the flowfield is predominately supersonic the transonic iterative technique is inefficient for the treatment of flows in this Mach number range. Hence, an intermediate method that marches in the supersonic zones and iterates in a localized region of subsonic flow would be an efficient technique for this problem. This type of procedure was first suggested privately to the author by South.[1] Recently, this type of technique was adopted by Shankar et al.[2]

Results of an Axisymmetric Study

The fully implicit marching method of Refs. 3 and 4 is used to solve the axisymmetric nonconservative full potential equation in a spherical coordinate system. For strong bow shocks, inaccuracies develop due to the nonconservative capture and smearing of these shocks. Hence, the bow shock is fit isentropically as a boundary (e.g., Ref. 5 or 6). The occurrence of a subsonic total Mach number region precludes the use of a marching scheme and an iterative technique must be used in the radial marching direction, Z. As a preliminary study, the conical solution was computed and held fixed at the apex or $r=0$, and the entire flowfield over the forebody shape was then computed by iteratively sweeping downstream using body-to-bow shock line relaxation. The Z derivatives must be modified to accommodate the iterative procedure. The radial Z second derivatives of the potential were computed using second-order accurate central difference formulas in subsonic zones. First derivatives were always central differenced. The details of the numerical scheme are presented in Ref. 6.

In general, the remainder of the body could be computed using the marching scheme. No attempts were made in this preliminary study to a priori define the zone of subsonic radial and total Mach number.

Figure 1 shows computed results for a 25-deg cone at $M_\infty = 1.401$ with an expanding afterbody initiated at $Z=0.2$ and terminating in a cylinder at $Z=0.3$. This solution was generated on a 60×45 (Y,Z) grid and took less than 1 min of CPU time on an IBM 3033. Figure 1a shows a Mach number contour plot. A significant portion of the conical flow at the apex contains subsonic flow. The conical transonic flow solution at the apex ($Z=0$) is used as the upstream starting condition. The interesting aspect of this solution is that little upstream influence occurs due to the presence of subsonic flow (Fig. 1). In fact, the sonic line attaches to the body at the point where the body slope first deflects. Figure 1b shows the surface pressure coefficient solution indicating that about five points upstream of the shoulder differ noticeably from the initial cone pressure. Reference 7 contains some Mach contour experimental data for cone cylinders under the same conditions but for a shoulder region of zero radius of curvature. The data also indicate that the upstream influence is very small. The present technique did not permit the calculation of transonic flow over cone cylinders with discontinuous curvature. It should be mentioned that the transonic cone solution was used as the starting potential for the forebody and is far from ideal as an initial guess. It initially violates the hyperbolic downstream condition but very quickly becomes supersonic downstream of the shoulder.

Figure 2 shows a series of fine mesh (60×97) solutions at $M_\infty = 1.55$ for a 20-deg supersonic cone (at the apex) with a gradual compression initiated at $Z=0.01$ and terminating at a specified deflection at $Z=0.25$. The compression surface is followed by an expanding afterbody which terminates in a cylinder at $Z=1.00$. These fine grid solutions were determined using a single mesh refinement. Some instabilities arose in the fine mesh solution in the vicinity of the downstream sonic line due to the abrupt finite difference switching at $M=1$. These

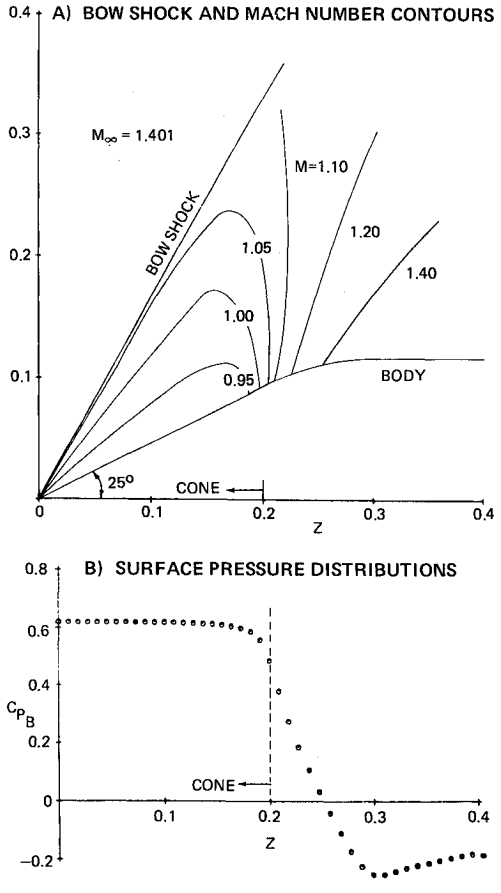

Fig. 1 Axisymmetric solution for a transonic 25-deg cone with an expanding afterbody at $M_\infty = 1.401$.

Received Aug 5, 1983; revision received Oct. 4, 1983. Copyright ©American Institute of Aeronautics and Astronautics, Inc., 1983. All rights reserved.

*Staff Scientist. Member AIAA.